Force-controlled 3D mechanical stretching to enhance the exosome secretion of bone mesenchymal stem cells for bone repair

Jie Wu a, b, c,1, Hao Wang d,1, Tao Sune, Qing Shie, Xie Chene, Yuanbo Qia,b,c , Sheng Tao b, a, c, Jiahua Zhaof*, Daohong Liu b, a, c*

a Department of Orthopedics, The First Medical Center of Chinese PLA General Hospital, Beijing 100853, People's Republic of China

b Department of Orthopedics, The Fourth Medical Center of Chinese PLA General Hospital, Beijing 100142, People's Republic of China

c Department of Orthopedics, The Eighth Medical Center of Chinese PLA General Hospital, Beijing 100091, People's Republic of China

d Department of Orthopaedics, Lanzhou University Second Hospital, No. 82 Cuiying Gate, Chengguan District, Lanzhou 730030, Gansu, People's Republic of China

e Intelligent Robotics Institute, School of Mechatronical Engineering, Beijing Institute of Technology, Beijing 100081, People's Republic of China

f Department of Thoracic Surgery, The Sixth Medical Center, Chinese PLA General Hospital, Beijing,100048, People's Republic of China

∗Corresponding authors at: Department of Orthopedics, Chinese PLA General Hospital, Beijing 100853, China.

E-mail addresses: jiahua301@163.com (J. Zhao) and domb@vip.sina.com (D. Liu)

1 These authors contributed equally to this work.

Preprint of Bio-Design and Manufacturing (unedited)

Abstract

Exosomes derived from bone marrow mesenchymal stem cells (BMSCs) show promising potential in the treatment of bone defects. However, their clinical application has been hindered by low yield and insufficient repair ability. Mechanical stimulation in 3D has been a well-known method to enhance exosome secretion, however, the traditional stimulation process was always achieved by controlling the displacement of manipulator, which may induce uneven loading distribution and degradation of stimulation strength. Here, we proposed a micro-stretching manipulator with a capacity of automatically controlling the stretching force applied to GelMA/HAMA hybrid hydrogel sheets containing BMSCs within an incubator. To ensure structural stability of the sheets after long-term stretching, the mixing ratio of GelMA and HAMA was optimized according to the mechanical property response of the sheets to cyclical loading. Subsequently, a force-controlled mechanical loading was applied to the BMSC-laden sheets in order to produce exosomes. Compare with the control for displacement, force-controlled loading has been demonstrated to provide a more stable force stimulation, thereby enhancing the secretion of exosomes. Furthermore, continuously stimulated exosomes have exhibited a more potent capacity in promoting the osteogenic differentiation of BMSCs and facilitating the repair of bone defects in a rat model. These findings suggest that force-controlled loading for cell-laden hydrogel offers a novel approach for the production of BMSC-exos and their application in bone repair.

Key words: exosomes, force control, mechanical loading, mesenchymal stem cells, bone repair

1 Introduction

Large bone defects, resulting from trauma, infection, tumors, and other etiologies, pose a prevalent and challenging clinical issue[1,2]. The traditional method of using autogenous bone grafts for filling has limitations, such as limited bone volume and complications at the donor site[3]. While artificial bone repair materials are an important resource for repairing bone defects, they lack biological activity and osteoinductivity.[4,5]. Bone mesenchymal stem cells (BMSCs) have become important seed cells in the field of tissue engineering due to their capability for self-renewal, multidifferentiation and paracrine activity[6]. In the study of the application of BMSCs in tissue engineering, several limitations have been identified, including a low survival rate after transplantation, tumorigenicity, and immunogenicity[7]. Recent studies have revealed that BMSC-derived exosomes (BMSC-exos) are capable of performing most of the functions of BMSCs. Furthermore, they exhibit no immunogenicity or risk of tumor formation, and offer the advantages of targeting, ease of use, and processability. Additionally, BMSC-exos play a crucial role in the treatment of bone-related diseases by maintaining bone metabolism homeostasis, modulating bone innervation, regulating immunity, and promoting vascularization[8,9]. It should be pointed out that the low yield presents a significant obstacle to the engineering application of exosomes.[10,11]. Studies have indicated that the production of exosomes can be enhanced by appropriate physicochemical stimuli.[11]. Due to the challenges in ensuring the biological safety of various biochemical stimuli, there is a growing focus on physical stimulation programs. The research conducted by Wang et al.[12]found that under cyclic stretching conditions, the secretion of exosomes from periodontal ligament cells increased by 30 times compared to static culture conditions. Mechanical stimulation plays an important role in the proliferation, differentiation and paracrine of BMSCs. Therefore, it is theoretically possible to achieve higher BMSC-exos production by appropriate mechanical stimulation. Meanwhile, the insufficient repair ability poses another challenge for the clinical application of exosomes.[8]. Mullen et al.[13] found that mechanical stretch stimulation can enhance the ability of exosomes to promote cell proliferation and myogenic differentiation by changing the composition of miRNAs contained in exosomes. Xiao et al.[14] found that BMSC-exos, following cyclic stretch treatment, were able to inhibit osteoclast generation by attenuating the activity of the NF-κB signaling pathway. Furthermore, the mechanical stimulation-induced BMSC-exos exhibited superior ability in inhibiting osteoporosis. Therefore, increasing the production and enhancing the function of exosomes through mechanical stimulation is helpful to realize the clinical application of exosomes, but there is still a lack of effective methods to achieve this goal.

Current research on the effects of mechanical stimulation on MSC differentiation and paracrine activity primarily focuses on 2D culture environments[13,15], but some studies have shown that the responses of cells to various stimuli in a 3D culture environment, which is more similar to the physiological state, are inconsistent with or even contrary to those in 2D culture[16-19]. Therefore, it is necessary to investigate the effect of mechanical stimulation on the secretion and function of BMSC-exos in 3D culture environment. Recently, a novel magnetically stretched cell-laden collagen hydrogel was developed to show enhanced osteogenic activity of mesenchymal stem cells-derived exosomes in 3D[20]. However, traditional mechanical loading methods for 3D-cultured cells are mostly based on elastic membrane platforms[21,22].The

Preprint of Bio-Design and Manufacturing (unedited)

expansion of the membrane allows for the straining of cell-laden hydrogel installed on the membrane, however, the resulting mechanical loading varies depending on the location of the cells encapsulated in the hydrogel[22]. Alternatively, a stretching apparatus can use mechanical grippers to stretch cell-laden hydrogel for mechanical loading. A uniform tensile force can then be applied along the stretched direction of the hydrogel[23]. Most of the current 3D mechanical loading methods are based on hydrogel deformation, with the degree of deformation being controlled by the displacement of the membrane and the grippers[21,22,24]. However, the mechanical properties of hydrogels can gradually weaken under displacement-controlled loading modes. Consequently, the mechanical force applied on cells due to hydrogel deformation may be attenuated accordingly. The maintenance of sustained force stimulation during long-term dynamic culture remains a challenge, potentially hindering the consistent attainment of a high yield of functionally enhanced exosomes. Therefore, it is necessary to adopt a mechanical loading model based on force control to further explore the effect of unattenuated force stimulation on the production and osteoinductive ability of BMSC-exos.

In this study, we have developed a force-controlled mechanical loading method to facilitate the production of BMSC-exos under long-term and constant force stimulation in 3D. The schematic of the whole method is shown in Figure. 1. BMSCs were encapsulated into a GelMA/HAMA hybrid sheet for 3D culture. A force-controlled loading instrument was established to dynamically stretch the sheet in an incubator environment. An optimal ratio of GelMA/HAMA was determined based on the response of the sheet's mechanical properties to dynamic stretching. Subsequently, a force-controlled mechanical loading was applied to the BMSC-laden sheet for a 7-day cell culture period. Based on this culture method, we investigated the impact of constant force stimulation on the amount of exosome secretion and its contribution to osteogenesis. The subsequent application in repairing rat bone defects further demonstrated that the combination of optimized 3D culture sheets and force-controlled stimulation can provide an effective method for the application of BMSCs-exos in the field of bone regeneration.

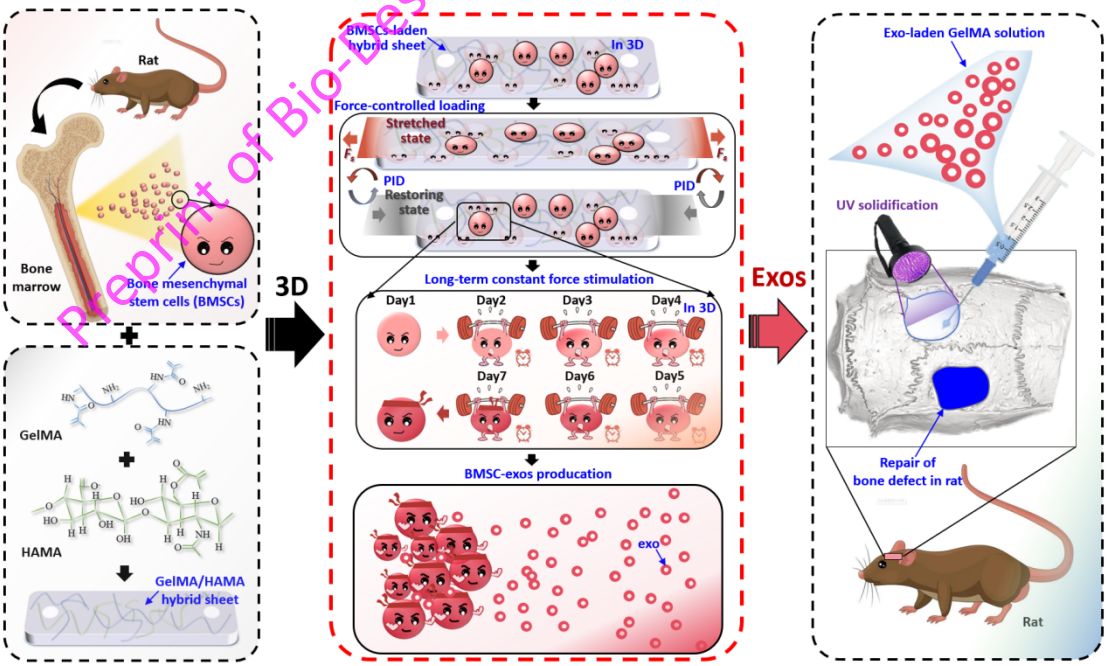

Figure. 1 Schematic of long-term force-controlled 3D mechanical stimulation to produce exosomes derived from BMSCs for repairment of bone defect

Preprint of Bio-Design and Manufacturing (unedited)

2 Methods

2.1 Cell culture and characterization of BMSCs

Sprague-Dawley rat BMSCs were obtained from OriCellBio (RASMX-01001). The expression of BMSC surface markers, including CD34 (Invitrogen, PA5-85917), CD45 (BioLegend, 2021205), CD90 (BioLegend, 202523) and CD105 (Invitrogen, MA1-19594), was analyzed using flow cytometry and FlowJo 10.0 software. Following the manufacturer's instructions, BMSCs were cultured in osteogenic induction medium, adipogenic induction medium, and chondrogenic induction medium (OriCellBio RAXMX-90021, RAXMX-90031 and RAXMX-90041) and stained with alizarin red, oil red O, and alcian blue to assess their differentiation ability.

2.2 3D culture of BMSCs

For the 3D culture, we used GelMA (EFL-GM-30) and HAMA (EFL-HAMA-150K) provided by Yongqinquan Intelligent Equipment Co., Ltd. (Suzhou, China). The composite hydrogel was prepared using the following concentrations: 5% w/v GelMA (G5 group), 5% w/v GelMA+0.1% w/v HAMA (G5H01 group); 5% w/v GelMA+0.3% w/v HAMA (G5H03 group); and 5% w/v GelMA+0.5% w/v HAMA (G5H05 group). The composite hydrogel was then dissolved by immersion in PBS containing the photoinitiator phenyllithium-2,4,6-trimethylbenzoyl phosphonate (LAP, 0.25% w/v), accompanied by shaking. After filtration of the composite hydrogel through a 0.22um filter, BMSCs were resuspended in the hydrogel with a cell density of approximately 1.0 × 106 mL-1 .

The 3D culture of BMSCs is conducted in a hydrogel sheet. To fabricate a hydrogel sheet compatible with our loading device, we utilized a template casting technique. This process began with the creation of an acrylic template featuring a concave structure, achieved through CNC machining. Subsequently, a PDMS mixture in a 1:10 ratio was poured into this template. Following a heating period of 4 hours at 60℃, the PDMS mold was successfully formed. We then injected 140 µl of cell-laden hydrogel into this mold and cured it using ultraviolet light. Due to the hydrophobic nature of PDMS, the hydrogel sheet could be easily removed from the template for further procedures. The cell-laden hydrogel sheet was then placed into a dish and complete medium was added before incubating it in an incubator.

2.3 Mechanical loading instrument

The mechanical loading instrument employed a two-probe configuration for stretching hydrogel as shown in Figure. S1. One of the probes, mounted on a linear actuator (AML40P) with a repeatability of ±0.2 µm, was the moving probe made of quartz (outer diameter: 1 mm; inner diameter: 0.6 mm). The other probe, mounted on a stepper motor (NSA12) with a minimum incremental movement of 0.2 µm, was the sensing probe also made of quartz (outer diameter: 0.7 mm; inner diameter: 0.5 mm). The deflection of the probe was captured by a digital camera (B011) operating at a frame rate of 15 Hz. Subsequently, using Python script (version 3.8), the deformation-related tensile force Fs was calculated and controlled through an in-house developed program. To ensure stability in culture conditions during stimulation, both probes and hydrogel were enclosed within a transparent operating chamber fabricated using 3D printing technology while being placed inside an incubator (H2300-HC2). Detailed experimental procedures are available in Supplementary Information Sections 1.1 and 1.2.

Preprint of Bio Design and Manufacturing (unedited)

2.4 Mechanical stimulation loading protocol

The hydrogel sheets, with or without BMSCs, were pre-cultured for 24 hours before being subjected to tensile mechanical stimulation. The loading parameters for displacement control loading (MD group) were set to maintain a distance control at 10% strain and a frequency of 1 Hz. In the force control group (MF group), force control was applied at the predicted Fs intensity (10% strain) with a frequency of 1 Hz. The static culture (M0 group) was utilized as the control group. All cultures, whether static or mechanically loaded, are placed in a incubator for cultivation and collected for analysis at the appropriate time points.

2.5 CCK-8 assay and Live/dead viability assay

To evaluate cell proliferation within various composite hydrogels, a CCK-8 kit (Dojindo, CK04-500) was utilized. On the 1st, 4th, and 7th days of cell culture, the original medium was replaced with complete medium containing 10% CCK-8. Following a 2-hour incubation in darkness, the medium was transferred to a 96-well plate. Absorbance at 450 nm was measured using an enzyme labeler. Each experimental condition was replicated across five wells, and the entire experiment was conducted five times to ensure reliability.

The viability of BMSCs in different composite hydrogels was assessed using a live/dead staining kit (Abbkine, KTA1001). After 7 days of culture, the hydrogels containing cells were washed three times with PBS. Subsequently, LiveDye/NucleiDye reagent, as recommended in the instructions, was added to each well. Following a 30-minute incubation, the culture plates were washed again and examined under a fluorescence microscope (Nikon, DS-Ri2).

In order to further investigate the impact of mechanical stimulation on the proliferation and viability of 3D-cultured BMSCs, we exposed the cells to various mechanical stimuli. On the 1st, 4th, and 7th days of mechanical loading, transfer the cell-laden hydrogel sheets of M0 group, MD group, and MF group to a 48-well plate and perform CCK8 assay and live/dead staining experiments following the above steps.

2.6 Cytoskeleton staining

To investigate the impact of mechanical stimulation on the morphology of BMSCs, FITC-labeled phalloidin (Solarbio, CA1620) and DAPI (Solarbio, CA1620) staining solution were used for cytoskeletal and nuclear staining, respectively. On day 7 of cell culture, the medium in the wells was aspirated and washed three times with PBS. Subsequently, fixation was performed using 4% paraformaldehyde for 30 minutes at room temperature followed by permeabilization with 0.5% Triton X-100 (Solarbio, T8200) for 15 minutes. The cytoskeleton was then stained with FITC-labeled phalloidin at the recommended concentration and incubated for 12 hours at 4°C in darkness before being rinsed twice with PBS. Nuclei were stained with DAPI solution for 10 minutes followed by another wash with PBS prior to observation under a laser confocal microscope (Leica, TCS SP8).

2.7 RNA-sequencing analysis

To further investigate the impact of mechanical stimulation on BMSCs, mRNA-sequencing analysis was conducted on cells from both the M0 group and MF group. Total RNA was extracted from the samples using TRIzol reagent(Tiangen Biochemical Technology, DP405-022) . The RNA was then assessed and quantified. Subsequently, RNA libraries were prepared and sequenced by

Preprint of Bio-Design and Manufacturing (unedited)

a commercial sequencing company using the Illumina NovaSeq™6000 platform. Sequencing data were filtered using Fastp (v0.14.0) software. The clean reads were then aligned to the reference genome and mapped with the reference coding gene set using HISAT2 (v2.2.0). Subsequently, StringTie (v2.2.1) was utilized to calculate the expression levels of genes. Differential expression analysis was conducted using Limma (v3.32.10), with a criteria for selecting differentially expressed genes as |log2FC|>=1 and p-Value<=0.05.Gene Ontology (GO) and Kyoto Encyclopedia of Genes and Genomes (KEGG) enrichment analyses of differentially expressed genes (DEGs) were performed using the R package clusterProfiler. Each group consisted of 3 biological replicates.

2.8 Extraction, identification and concentration analysis of exosomes

After 7 days of mechanical stimulation, the medium was replaced with exosome-depleted medium and the culture was continued for an additional 48 hours. The supernatant was collected and cellular debris was eliminated through centrifugation at 300×g for 10 minutes followed by centrifugation at 2000×g for 20 minutes. Subsequently, the supernatant underwent centrifugation at 10,000×g for 30 minutes, followed by filtration using a filter with a pore size of 0.22 μm, and ultracentrifugation at 100,000×g for 70 minutes. Finally, the cells were washed twice with large volumes of PBS and subjected to another round of centrifugation at 110,000×g for an additional period of 70 minutes in order to eliminate any contaminating proteins. All these procedures were conducted at -4°C. The prepared exosomes were resuspended in PBS and stored at -80°C.

The morphology of exosomes was observed using a transmission electron microscope (HT7700, Hitachi). Western blotting was used to verify exosome-specific surface markers (CD9, CD81, TSG101 and Calnexin). Exosomes were lysed using RIPA (R0010, Solarbio), and the BCA assay (P0012, Beyotime) was performed to determine the protein concentration. The protein samples were normalized and denatured at 95 ℃ with SDS-PAGE loading buffer (P0015, Beyotime) for 5 minutes. Subsequently, the proteins were separated by a 4－20% Bis-Tris SDS-PAGE gel and transferred onto polyvinylidene fluoride (PVDF) membranes (1620177, Bio-Rad). The membranes were blocked with EveryBlot Blocking Buffer (12010020, Bio-Rad) for 10 minutes at room temperature and then incubated with primary antibodies overnight. Following this, the membranes were washed three times for 10 minutes each with TBST and incubated with the corresponding secondary antibodies. After another three washes of 10 minutes each with TBST, Clarity Western ECL Substrate (1705060) was applied and images were captured using a G:BOX Chemi XX6 gel doc system (Syngene). Finally, the images were further processed using Image J. The size and concentration of BMSC-exos was measured by nanoparticle tracking analysis (NTA) software using a NanoSight NS500 instrument (Malvern Instruments, Malvern, UK). To account for variations in the number of cells between different groups, the total number of BMSC-exos was normalized by dividing it by the number of BMSCs to calculate the average number of exosomes secreted per BMSC.[25].

2.9 Cellular uptake of sEVs

BMSCs were seeded into 8-well chamber slides at a density of 1.5×104 cells/well and cultured overnight in an incubator. BMSC-exos collected from groups M0, MD, and MF were labeled using an exosome membrane labeling kit (Dojindo, Japan) following the manufacturer's instructions.

Preprint of Bio Design and Manufacturing (unedited)

The labeled BMSC-exos were then resuspended in exosome-free complete medium to a concentration of 1.5×108 particles/ml. Subsequently, 300 μl of the medium containing labeled exosomes was added to each well and incubated in the dark for 12 hours. After washing three times with PBS, the cells were fixed, permeabilized, and stained with FITC-labeled phalloidin for the cytoskeleton and DAPI for the nucleus. The stained cells were observed under a confocal laser microscope (Leica, TCS SP8).

2.10 qRT–PCR analysis

BMSCs were cultured in a 3D environment using exosome-free complete medium. The control group received the addition of 10% PBS, while the M0, MD, and MF groups received the addition of 10% BMSC-exos (1×109 ml) extracted from their respective groups (M0, MD, and MF). The positive control group, named as group CI, was chemically induced with osteogenic induction medium. The expression of osteoblast-related genes in BMSCs from the control, M0, MD , MF and CI groups was evaluated using qRT–PCR. On the 7th and 14th days of culture, cell-laden hydrogel sheets from the various treatment groups were harvested. The hydrogel were lysed using lysates (Yongqinquan Intelligent Equipment, LS-001) according to the provided instructions. Total RNA extraction from BMSCs was performed following the guidelines for the TRIzol reagent. Reverse transcription to cDNA was carried out using the HiScript III 1st Strand cDNA Synthesis Kit (Nanjing Nuoweizan, R312-01) with gDNA Eraser, strictly adhering to the kit's protocol. qRT–PCR was conducted on a real-time PCR system (Applied Biosystems, ABI 7500) using Universal SYBR Green Supermix (CoWin Biosciences, CW0957). The primers used are listed in Table S1, with GAPDH serving as the normalization control. Each sample was tested in triplicate, and the experiment was replicated three times. Data analysis was performed using the 2^-ΔΔCT method.

2.11 ALP staining and alizarin red staining

Alkaline phosphatase (ALP) staining and alizarin red staining were used to detect the ability of BMSC-exos to promote osteogenic differentiation of BMSCs in 3D. According to different treatment methods, the samples were divided into the control, M0, MD, MF, and CI groups. On the 7th day of culture, cell-laden hydrogel sheets were washed with PBS and fixed with 4% paraformaldehyde at room temperature for 20 minutes. After washing again, the BCIP/NBT kit (Beyotime Biotechnology, C3250S) was applied for ALP staining. After incubation for 2 hours at room temperature in the dark, the cells were washed again and observed with a stereomicroscope (Nikon SMZ25). On the 14th day of culture, the cells were washed and fixed according to the above steps. Then, the cells were stained with alizarin red (OriCellBio, ALIR-10001), incubated at room temperature for 5 min, washed again and observed with a stereo microscope. Image J (version 1.8.0) software was used to calculate the area of the positive region.

2.12 Animal experiments

A rat calvarial defect model was utilized to assess the osteogenic potential of BMSC-exos under various treatment conditions in vivo (Figure 6a). All animal experiments were carried out in strict accordance with protocols approved by the Chinese PLA General Hospital. Twenty male Sprague–Dawley (SD) rats (350-400 g, aged 10-12 weeks) were obtained from SPF Biotechnology Co., Ltd. (Beijing, China). The animals were housed in the animal laboratory of the 8th Medical Center of

Preprint of Bio Design and Manufacturing (unedited)

the PLA General Hospital under a 12-hour dark/light cycle with ad libitum access to food and water. According to the different treatments, the animals were divided into four groups: the defect group (bone defects area left empty, without implantation), M0 group, MD group, and MF group (bone defects area was implanted with a hydrogel containing BMSC-exos from the M0 group， MD group and MF group, respectively). Isoflurane inhalation anesthesia was used. After successful anesthesia, the hair from the eye to the back end of the skull was shaved, the area was disinfected with sterile towels and 75% alcohol, and a 2 cm longitudinal incision was made along the midline of the skull. The skin, subcutaneous tissue and fascia were cut one by one to expose the skull. A dental trephine was used to carefully drill two full-thickness bone defects approximately 5 mm in diameter into the parietal bone on both sides of the midline of the skull. According to the literature report, the degradation time of GelMA-60 (EFL-GM-60) at a concentration of 10% w/v in vivo is approximately one month[26]. In this study, GelMA-60 was utilized as a carrier to sustain the activity of BMSC-exos in the bone defect area. To assess the variance in bone repair capability of BMSC-exos obtained through different pretreatments, 20ul of hydrogels containing BMSC-exos with various pretreatments (1.0×108 particles) were injected into the bone defect area. Subsequently, the hydrogel was photocrosslinked and cured. The incisions were sutured layer by layer. After awakening from anesthesia, the rats were transferred to a clean cage for independent feeding and given free access to food and water. Finally,100000U of penicillin sodium was injected intramuscularly for 3 consecutive days after operation to prevent infection.

2.13 Micro-CT

At the 8th week post-operation, the rats were anesthetized with isoflurane inhalation and euthanized by tail vein air embolization. Subsequently, the skulls were dissected and fixed in 4% paraformaldehyde. The skull specimens were scanned using a micro-CT system (Bruker SkyScan 1276) with a scanning voltage of 70 kV, current of 200 μA, resolution of 6.5 μm, and exposure time of 350 ms. The original images were reconstructed using NRecon (V1.7.4.2, Bruker, Germany) for three-dimensional visualization. CTAnalyzer (1.20.3.0, Bruker, Germany) was utilized to analyze the region of interest (ROI). Parameters such as total volume (TV), bone volume (BV), volume ratio (BV/TV), trabecular number (Tb.N), trabecular thickness (Tb.th), and structure model index were calculated by the software.

2.14 Histological staining

After conducting micro-CT analysis, the skull specimens from each group were decalcified in a 10% EDTA solution, embedded in paraffin, and sectioned at 5 μm. The sections underwent hematoxylin-eosin (HE) and Masson staining and were observed using optical microscopy (Leica, Aperio GT450).

2.15 Statistical analysis

GraphPad Prism 9.0 software was utilized for data plotting and statistical analyses. All values are presented as the mean ± standard deviation. One-way ANOVA was conducted to compare multiple groups, and an unpaired two-tailed Student's t test was performed to compare two groups, with a significance level of $p < 0.05$.

Preprint of Bio Design and Manufacturing (unedited)

3. Results

3.1 Stretching culture instrument for force-controlled strain application on sheets

The implementation of mechanical loading on the sheets was facilitated by a stretching culture instrument with the capacity of real-time stretching force control. As illustrated in Figure. 2(a) and Figure. (b), the instrument consisted of a two-probe actuator and a microscope camera, all of which could run steadily in an incubator environment (37oC, 5% CO2). The two-probe actuator consisted of a sensing probe and an actuating probe, which were horizontally positioned above the culture media surface of the Petri dish. Two microposts installed on the front ends of the two probes were respectively inserted into the two mounting holes in the sheet. When the actuating probe moved away from the sensing probe, the sheet could be stretched along its long axis. Stretching force Fs was uniformly delivered from the end of the sheet fixed at the actuating probe to the other end fixed at the sensing probe, and then the sensing probe could generate a flexing deformation x that could be recorded by the camera mounted above the probe to calculate Fs. To achieve control of Fs during stretching, the system computed the deviation e between the measured Fs and the expected force Fcmd in real time and fed it into the PID controller. Subsequently, the output value from the PID controller was transmitted from the PC to the motor controller to regulate the moving distance Lm of the actuating probe. Such a control method allowed the Fs to constantly match the Fcmd in long-term cell culture. The cyclical stretching process in a incubator was also shown in Video S1.

We used 5% w/v GelMA and 5% w/v GelMA mixed with 0.1, 0.3 and 0.5% w/v HAMA to form four groups (G5, G5H01, G5H03, and G5H05) for the fabrication of rectangular hydrogel sheets. The experimental results showed that the four groups of sheets could all be easily fabricated by the traditional PDMS template method (Figure. S2). The morphology of the resulting sheets are shown in Figure. 2(c); two mounting holes at both ends of the sheets were created for subsequent mechanical loading. The BMCSs used in this study had tri-lineage differentiation ability and expressed MSC surface markers (Figure. S3). Furthermore, BMSCs were embedded in the four sheets at a density of 1.0×106 cells/ml, forming a 3D culture environment. 7-day static cell culture experiments were conducted, and the CCK 8 results (Figure. S4) demonstrated that G5 exhibited the most rapid cell proliferation among all the groups. Additionally, it was observed that there was a noticeable decrease in the cell proliferation rate with increasing concentrations of HAMA. Live/dead staining results (Figure. 2c) showed that the cell viability in all groups exceeded 95%, suggesting that the resulting sheets did not exhibit pronounced cytotoxicity. Furthermore, to apply mechanical stimulation to BMSCs encapsulated in the sheets, the sheets were cyclically strained along their long axis by two stretching methods. The first method was distance-controlled strain during each loading cycle, in which the stretched distance of the sheets was kept constant regardless of the change in the internal stress σ in the sheets. The second method was force-controlled strain during each loading cycle, in which a constant stretching force was maintained through the whole sheet without consideration of dimensional changes of the sheet.

Preprint of Bio Design and Manufacturing (uncedited)

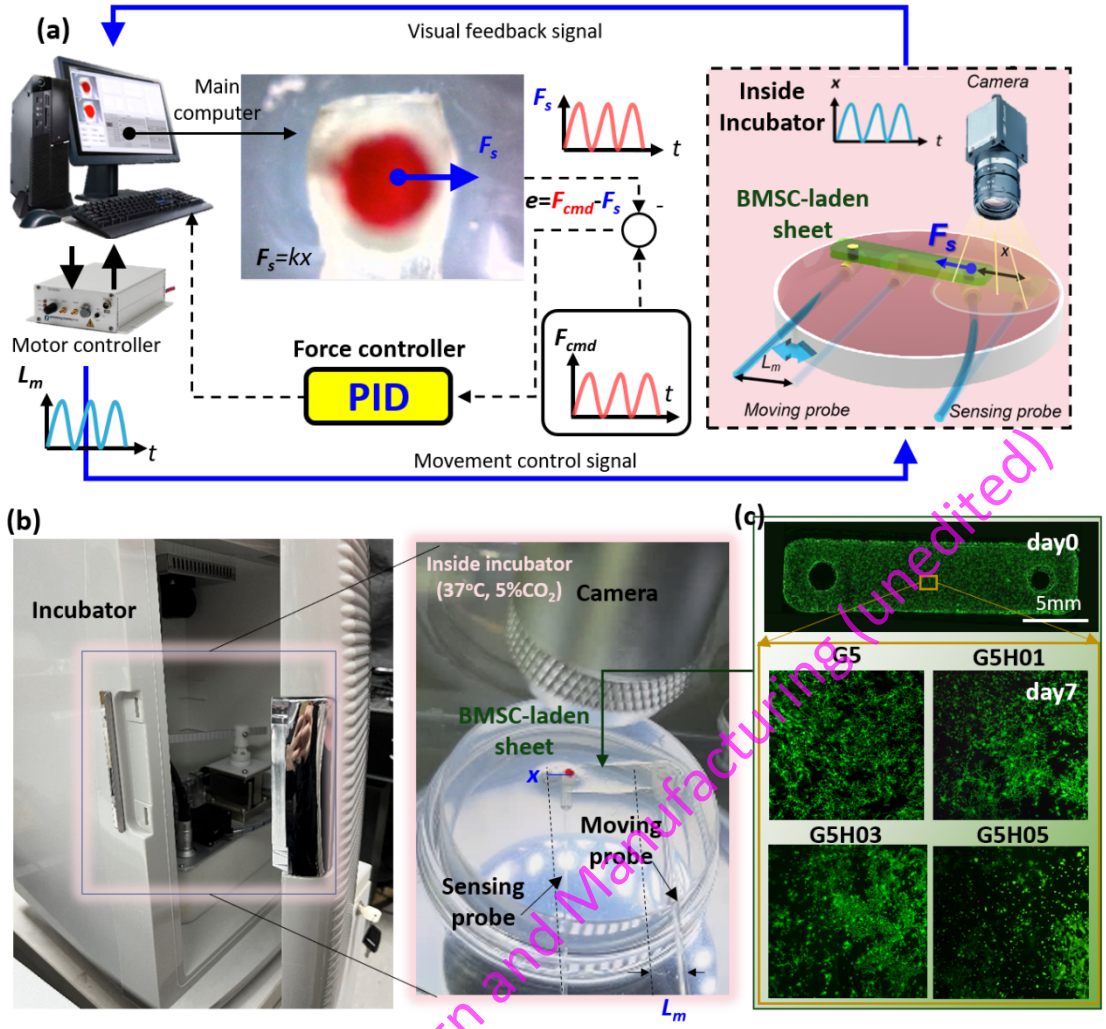

Figure. 2 Force-controlled mechanical loading system. (a) Schematic of the stretching culture instrument with the capacity of real-time stretching force control. (b) Physical picture of the instrument in an incubator. (c) Rectangular GelMA/HAMA hydrogel sheet for 3D BMSCs culture

Preprint of Bio-Design and Manufacturing (unedited)

3.2 Response of sheets to force-controlled strain application

We conducted a simulation using COMSOL to evaluate the effect of these two loading methods on the σ in the sheets when stretched to 10% amplitude, as depicted in Figure. 3(a) and Video S2. The behavior of the sheets was modeled using a viscoelastic model. It is generally observed that when the loading time t surpasses three times the time constant (3τ), the creep or stress relaxation of the viscoelastic material approaches a stable state. Accordingly, we simulated and analyzed the stress σ distribution from t=0 to t=3τ under force-controlled loading and displacement-controlled loading. The simulation results indicated that the maximum stress in the hydrogel sheet, irrespective of the control method, occurred at the micropillar contact point, while the strain in the central region remained almost uniform. However, under force-controlled loading, the hydrogel sheet moved Δ more distance than under displacement-controlled loading. Further extracting the σ inside the hydrogel sheet along the A-B line for comparison, it was observed that σ started to rise from point A and remained basically constant at the position 2 mm away from point A, after which σ started to fall from the position 2 mm away from point B until point B was close to 0. When the force was controlled, looking at the part marked by the

dotted line in the middle part of the A-B line, σ remained almost constant from t=τ to 3τ. However, without force control, from t=τ to 2τ, σ decreased at first but remained unchanged from 2τ to 3τ, indicating that after stress relaxation, the hydrogel sheet tended to be stable. The simulation results showed that compared with distance-controlled loading, force-controlled loading could effectively prevent stress decay to provide more stable force stimulation during the whole process of cell culture.

Furthermore, cell-free sheets in the four groups were cyclically strained by the proposed system, and the real-time change in Fs and the sheet strain ε were recorded to analyze the response of the sheets to the two stretching methods. Before testing, we first determined the magnitude of Fs when the four different sheets were statically stretched to produce 10% strain, and then the Fs was used as the Fcmd for cyclic stretching at a frequency of 1 Hz. The Fcmd corresponding to the four sheets was ~0.5mN, ~1.1mN, ~5.7mN, and ~10.3mN, respectively. The displacement-controlled and force-controlled loading methods were applied to the four sheets. Under force control, the measured Fs of the four sheets basically fluctuated around the Fcmd, as indicated by the blue curves in Figure. 3(b). However, under displacement control, the Fs gradually decreased in the initial phase (~300 s) and then tended to stabilize at ~70% of the original Fs, as indicated by the red curve in Figure. 3(b). The decay of Fs under displacement control shows that the viscoelastic hydrogel sheet undergoes a stress relaxation process. The corresponding ε values of the four sheets under force control are shown in Figure. 3(c). The initial ε of the hydrogel sheets reached approximately 10% and then continuously increased with progressive dynamic stretching. Furthermore, the composite modulus E* in the different groups at 1 Hz can be calculated by σ and ε. The composite modulus E* in the four groups was 0.8 kPa, 2.0 kPa, 10.6 kPa and 17.0 kPa, respectively. Compared with data reported in related studies[27], the measured moduli are largely consistent, indicating the accuracy of the measurement system.

When the Fcmd was set as the original Fs under 20% and 30% amplitude strain, a similar sheet response could also be achieved in all four sheets. However, while there was an increase in the sheet creep distance with increasing strain, there was no significant difference in the decay time of Fs. After continuous mechanical stretching in the incubator for approximately 5 hours, the morphology of four sheets was shown in Figure. 3(d). The sheet in G5 showed structural collapse due to the combined effect of swelling and low mechanical strength. When 0.1% HAMA was added, the morphology of the hydrogel remained nearly intact; however, there was an obvious tendency toward collapse, indicating that the sheet in G5H01 may have difficulty maintaining its structure for 14 days of dynamic stretching during cell culture. When the content of HAMA was increased to 0.3%, the sheet still maintained its original shape. In the cell-free state, the structure of the hydrogel sheet remained stable after force-controlled cyclical stretching for 24 hours. However, when the concentration of HAMA reached 0.5%, internal fracturing of the hydrogel sheet occurred after continuous mechanical loading for approximately 2 hours, and the original morphology could not be maintained. Therefore, here, we chose the sheet in G5H03 group as the vehicle for long-term force-stimulated 3D cell culture.

Preprint of Bio Design and Manufacturing (unedited)

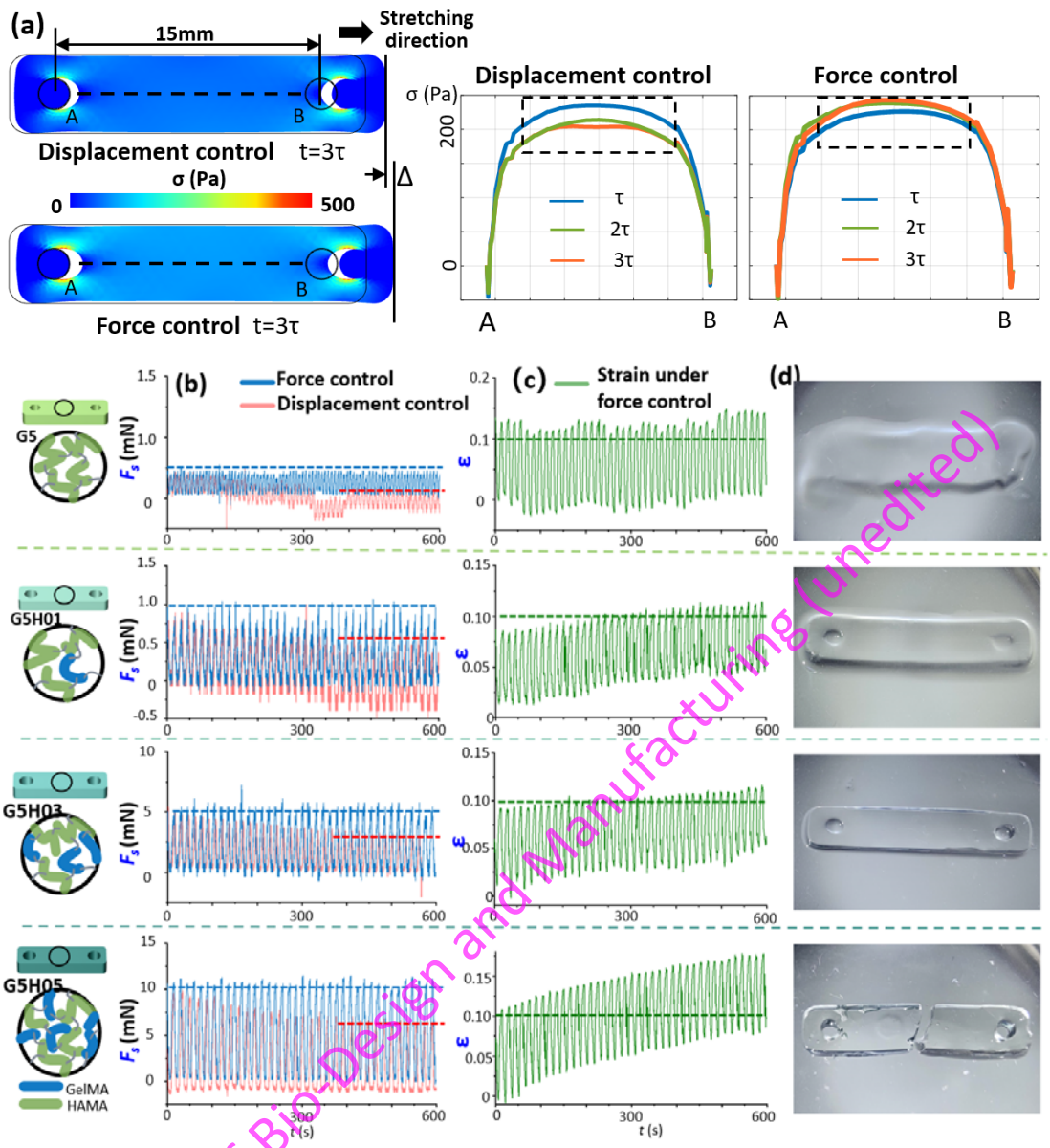

Figure. 3 Response of the sheet on mechanical loading. (a) Simulation for stress distribution throughout the sheet under two loading modes. (b)Time-dependent change of Fs under force control and displacement control for four sheets, respectively. (c) Time-dependent change of stain under force control for four sheets, respectively. (d) sheet morphology after cyclically stretching in incubator.

Preprint of Bio-Design and Manufacturing (unedited)

3.3 Response of BMSCs encapsulated in sheets to force-controlled strain application

BMSCs were encapsulated into the G5H03 hydrogel sheet, and then force stimulation was applied to the sheet by the stretching culture instrument for a long period. The Fs-induced mechanical loading schematic is shown in Figure. 4(a). The first day was devoid of mechanical stimulation to establish stable adhesion between BMSCs and the inner network of the sheet. Commencing on the 2nd day, Fs was applied at a frequency of 1 Hz for 20 minutes at a three-hour interval was initiated and maintained throughout the remainder of the 7-day culture period. The strain of the sheet was kept at 10% amplitude for displacement control (MD), and the Fcmd was set as the Fs under the initial strain at 10% amplitude for force control (MF). Figure. 4(b) shows the

time-dependent change in Fs under the two loading methods. For MF, Fs remained stable over the 14-day culture period, as delineated by the light blue curve. Conversely, for MD, there was a progressive decrease in Fs due to the effect of stress relaxation, as depicted by the sky blue curve. Furthermore, the BMSC-free sheet was used as a control group to evaluate the effect of cell activity on force stimulation. The trend of change in the Fs of the BMSC-free sheet was consistent with that of the BMSC-laden sheet; however, the diminution of the Fs in the BMSC-free sheet was less severe than that in the BMSC-laden sheet, as showed by the red curve. This discrepancy is likely due to the secretion of various enzymes by BMSCs greatly accelerating the degradation of GelMA such that the mechanical properties of the sheet become too weak to generate enough deformation to maintain the Fs.

To further evaluate the growth of BMSCs in the sheets, we set up three groups responding to three stimulation conditions: static culture (M0), MD and MF. Based on the CCK-8 method, the cell proliferation rate in the three groups was quantitively analyzed, as shown in Figure. 4(c). The M0 group exhibited the lowest rate of cell proliferation, while increased cell proliferation was observed in the other two groups. Specifically, BMSCs in MF group exhibited more rapid proliferation than those in the MD group on days 4 and 7, respectively. This result shows that force-controlled loading methods is a better strategy for cell growth than displacement-controlled loading methods. Subsequent live/dead staining experiments affirmed that cells maintained high viability, and the change in cell density during 7 days of cell culture further showed that the measurement of the cell proliferation rate was accurate. Cytoskeleton staining revealed that the cells in the M0 group predominantly aggregated on the hydrogel surface, exhibiting a morphology akin to that observed in 2D culture. Notably, little cell growth was observed within the hydrogel, corroborating the observations from live/dead staining. In contrast, mechanical stimulation resulted in a more uniform dispersion of cells, with a dendritic morphological extension and evident cellular interactions. Notably, the MF group showed higher cell densities than the MD group and cellular growth exhibited a directional pattern, characterized by cytoskeletal extension aligning with the direction of mechanical stimulation (Figure. 4d). mRNA sequencing revealed a significant number of differentially expressed genes (DEGs, Figure. S5a), with 914 genes up-regulated and 863 genes down-regulated (Figure. S5b). The clustering heatmap of DEGs clearly demonstrates the distinct separation between the MF group and the M0 group (Figure. S5c), validating the reliability of the differential expression analysis results. GO enrichment analysis indicates that these DEGs are predominantly enriched in biological processes such as extracellular matrix organization, extracellular structure organization, external encapsulating structure organization, and cell-substrate adhesion (Figure. 4e). KEGG enrichment analysis suggests that DEGs are primarily involved in signaling pathways including Focal adhesion, MAPK signaling pathway, and PI3K-Akt signaling pathway (Figure. 4f).

Preprint of Bio Design and Manufacturing (uncedited)

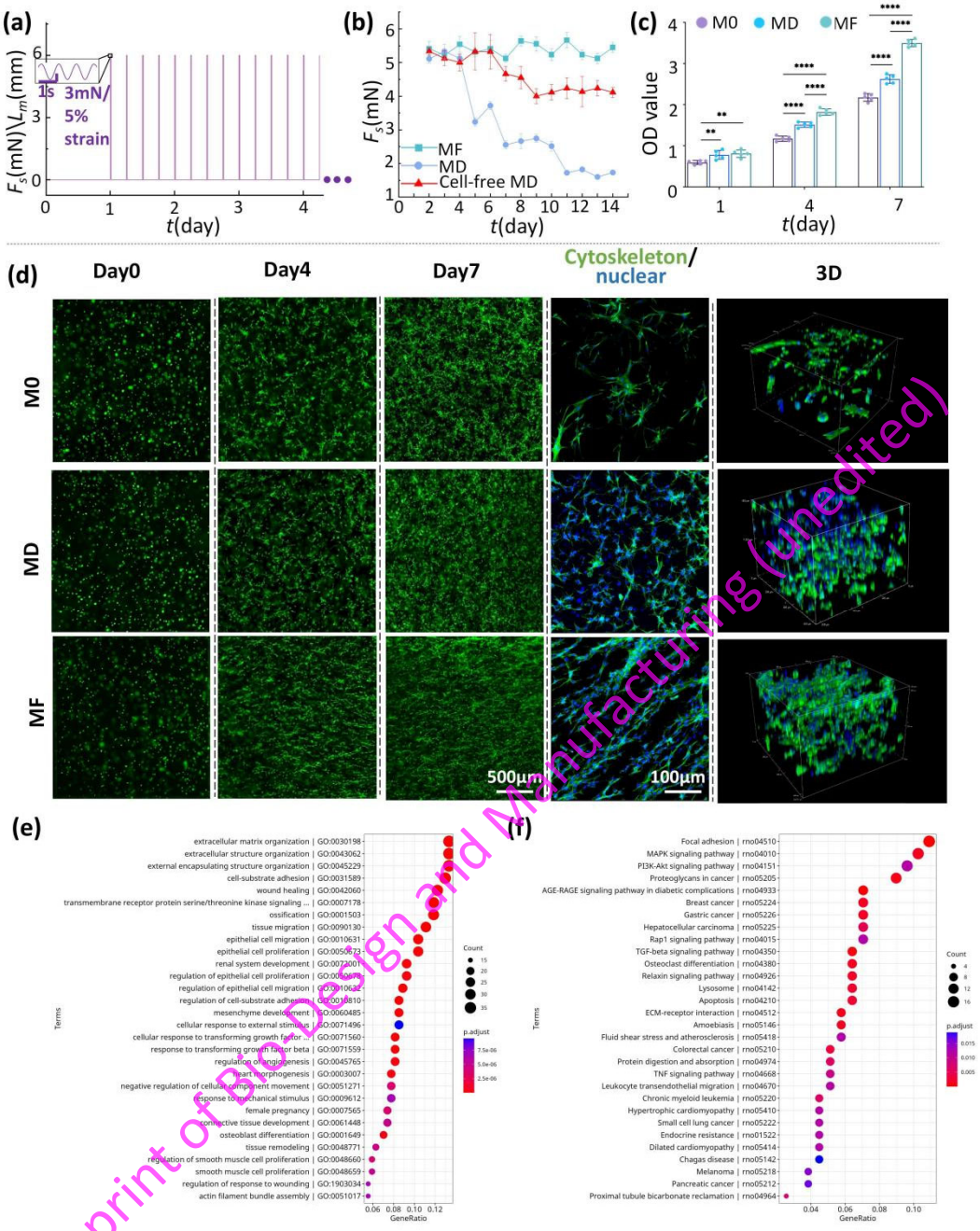

Preprint of Design and Manufacturing (unedited)

Figure. 4 Response of BMSCs encapsulated in the sheets to mechanical loading. (a) Mechanical loading strategy. (b) Time-dependent change of Fs under different loading modes. (c) Effects of three loading modes on the proliferation of the encapsulated BMSCs (**P < 0.01; ****P < 0.0001). (d) Live/dead staining of BMSCs in different mechanical loading groups (Green: live cells; red: dead cells) at 0, 4, and 7 days and cytoskeleton staining (Green: Factin strained with FITC-phalloidin; blue: nucleus stained with DAPI) of BMSCs in different mechanical loading groups on the 7th day of culture. (e) GO enrichment analysis of DEGs. (f) KEGG enrichment analysis of DEGs.

3.4 Mechanical stimulation promoted the secretion and functionalization of BMSC-exos

The process of BMSC-exos production in each group is shown in Figure. 5. The results of

transmission electron microscopy demonstrated that the three groups of exosomes showed typical dish structures, and no significant differences were observed in morphology (Figure. 5b). We identified the surface markers of the extracted exsomes by Western blot. Exos-specific markers CD81, CD9 and TSG101 were positively expressed in all the three groups of BMSC-exos, but Calnexin was not expressed (Figure. 5c). NTA results (Figure. 5d) showed that the particle sizes of the three groups of BMSC-exos were consistent with the distribution characteristics of exosomes. These results confirmed the successful extraction of BMSC-exos. We found that mechanical stimulation could significantly increase the secretion of BMSC-exos. The secretion of BMSC-exos in the MD and MF groups was significantly higher than that in the M0 group, and the secretion of BMSC-exos in the MF group was the highest, about 3.3 times that in the MD group and 8.5 times that in the M0 group (Figure. 5e). From the cellular uptake experiments, red-labeled exos were observed around the nucleus in all three groups, indicating that all three groups of BMSC-exos could be normally taken up by BMSCs (Figure. 5f). In the MF group, more BMSC-exos accumulated around the nucleus, suggesting that BMSC-exos produced by continuous and stable mechanical stimulation were more likely to be taken up by BMSCs. By fluorescence microscopy, we also found that the BMSC-exos could be evenly encapsulated within the hydrogel (Figure. 5g).

Preprint of Bio-Design and Manufacturing (unedited)

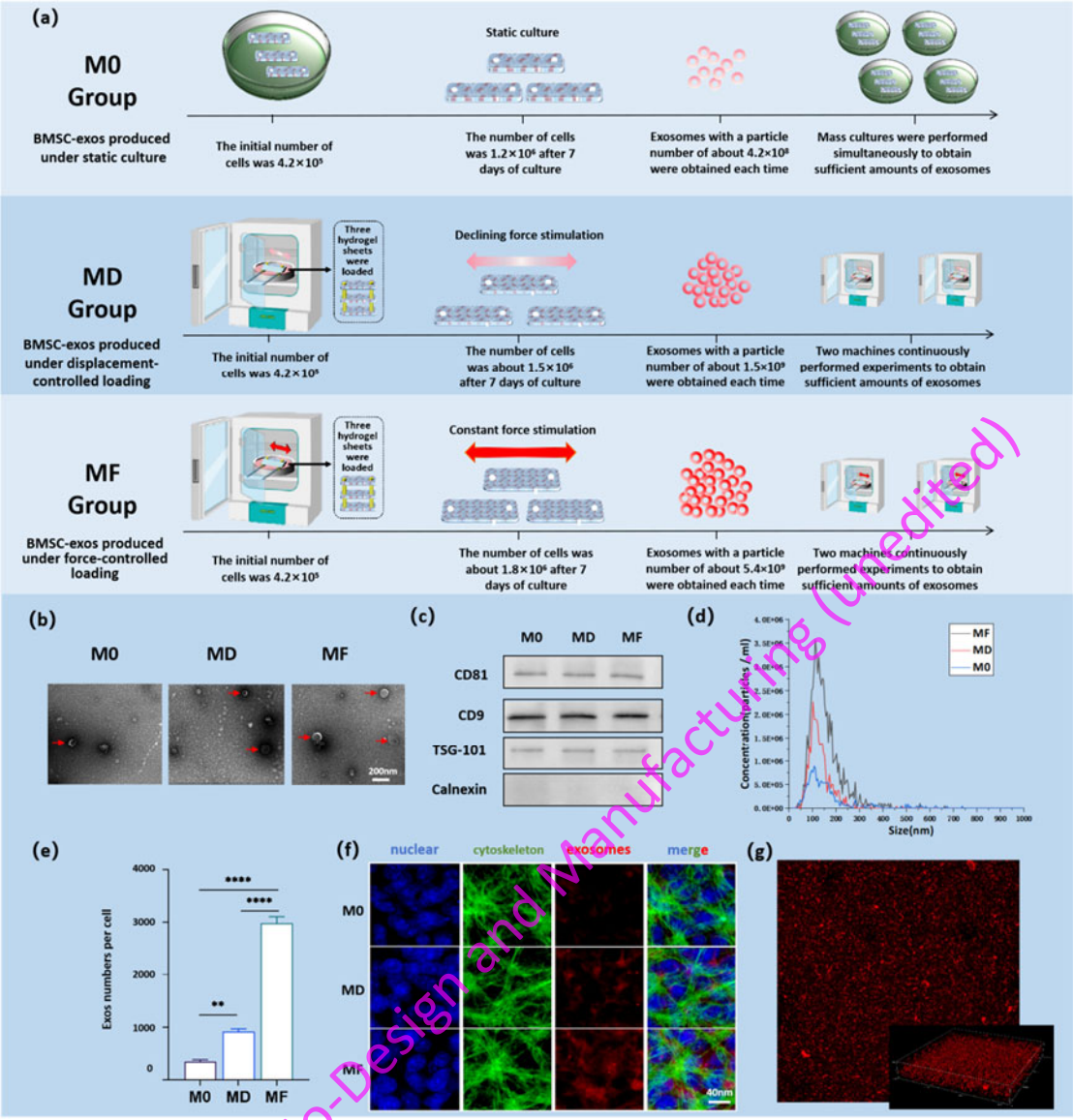

Figure. 5 Extraction and identification of BMSC-exos. (a) Schematic representation of BMSC-exos production in different groups. (b) TEM images of BMSC-exos secreted in M0, MD and MF groups. (c) The surface markers CD81, CD9, TSG-101, and Calnexin of BMSCs and BMSC-exos in M0, MD, and MF groups were identified by Western-blot. (d) Representative size distribution of BMSC-exos in M0, MD and MF groups. (e) Number of BMSC-exos secreted by each cell in M0, MD, and MF groups. (f) Fluorescence images of cell uptake of BMSC-exos from M0, MD, and MF groups. (g) Fluorescence image of exosomes uniformly distributed in the hydrogel.

Preprint of Bio-Design and Manufacturing (unedited)

To evaluate whether BMSC-exos induced by mechanical stimulation have a better ability to promote osteogenic differentiation, we performed 3D coculture of BMSCs and BMSC-exos. qRT–PCR analysis was used to measure the expression of osteogenic genes. By the 7th day of cultivation, the expression levels of the osteogenic-related genes RUNX2 (Figure. 6a), ALP (Figure. 6b), OPN (Figure. 6c), and OCN (Figure. 6d) in the MF group were significantly higher than those in the M0 and MD groups. This trend still existed on the 14th day. At the two selected time points, the expression of osteogenic-related genes in the MF group was close to that in the CI group. These results suggest that the constant force stimulation applied in the MF group could promote

the production of exosomes with stronger osteogenic capacity and has similar effects to chemical induction. We also observed that the expression of osteogenic genes in the MD group was higher than that in the M0 group. However, it was still lower in the MD group than in the MF group, indicating that displacement-controlled mechanical loading could enhance the osteogenic ability of BMSC-exos, but not to the same extent as force-controlled loading.

To further investigate the osteogenic induction ability of BMSC-exos induced by mechanical stimulation, we conducted ALP staining and alizarin red staining assays. It can be seen from the statistical results of ALP staining (Figure. 6e), prominent ALP-positive area were observed in the MF group and the CI group on the 7th day of culture, with no significant difference in the extent of staining between these two groups. Conversely, the M0 group displayed scarcely any ALP-positive area. The ALP-positive area in the MD group was higher than that in the M0 group, but lower than that in the MF and CI groups. Furthermore, the statistical results of alizarin red staining (Figure. 6f) revealed calcium nodule deposition in the MF and CI groups on day 14, while no obvious calcium nodule staining was observed in the M0 group. Some areas of calcium nodule staining could be observed in the MD group, but less so than in the MF and CI groups. Representative images of ALP and alizarin red staining are shown in Figure. 6(g) and Figure. 6(h) respectively.

Preprint of Bio-Design and Manufacturing (uncited)

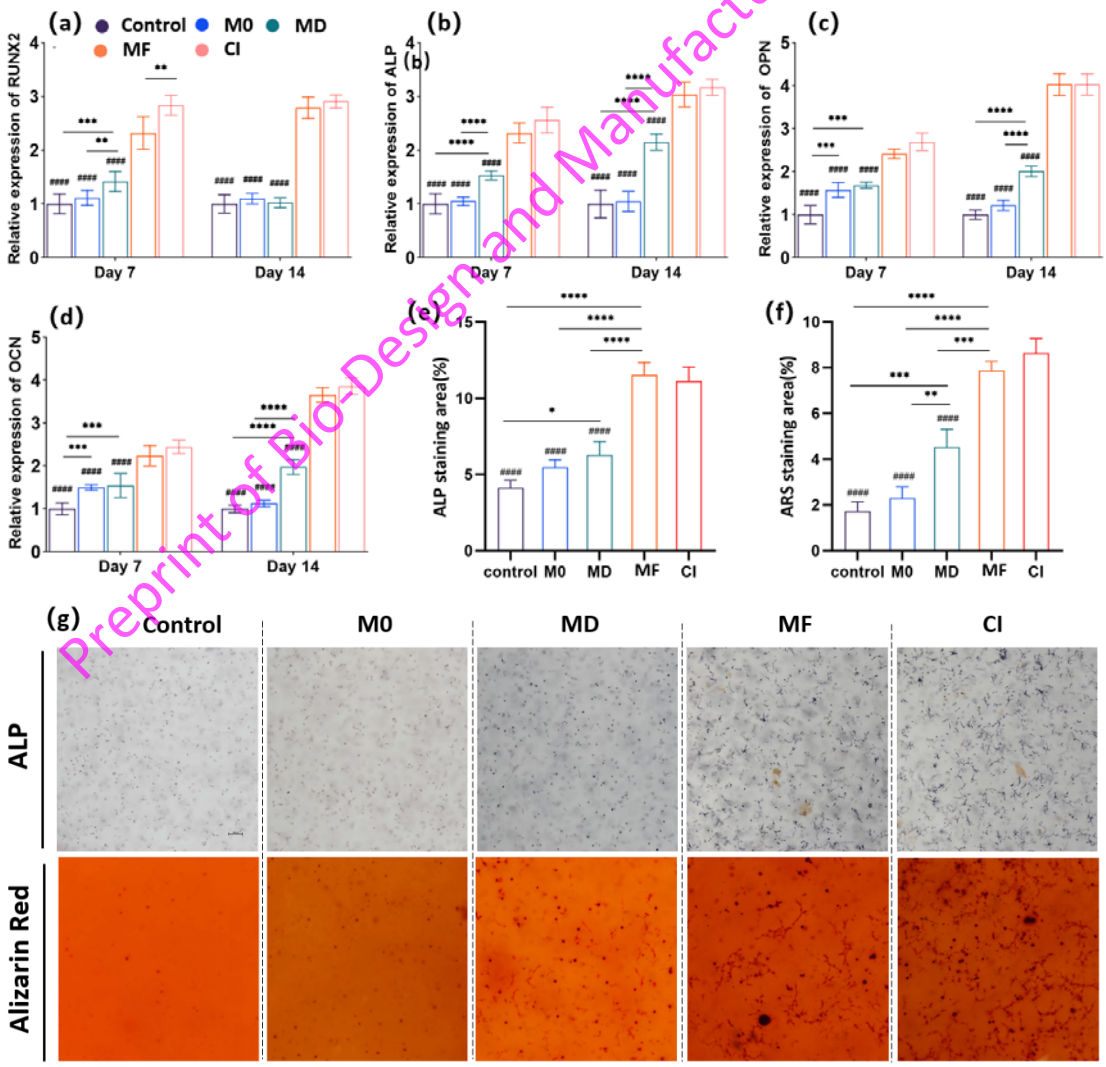

Figure. 6 Osteogenic differentiation of BMSCs induced by BMSC-exos from different treatment groups. (a-d) Expression of osteogenesis-related genes in each group on the 7th and 14th day of culture. (e-f) Quantitative analysis for positive areas of ALP staining and Alizarin Red staining, respectively. (g-h) ALP and Alizarin Red staining images of BMSCs. (*P < 0.05;**P < 0.01;***P < 0.001; ****P < 0.0001; #### compare to MF and CI groups, p< 0.0001).

3.5 Constant force stimulation induced BMSC-exos shows strong osteoinductivity

The 5-mm bone defect we constructed was a critical bone defect in rats, which would be unlikely to self-repair without intervention. Therefore, such rat model was utilized to verify the capacity of the constant force stimulation induced BMSC-exos to repair the bone defect, as shown in Figure.7(a). Additionally, three other groups were included: the defect group, M0 group, and MD group. Micro-CT results obtained at the eighth week postoperation revealed that the defect group (Figure. 7b) exhibited a lower bone volume fraction (Figure. 7f), trabecular thickness (Figure. 7g), and trabecular number (Figure. 7h), significantly lagging behind both the two stimulated BMSC groups. The M0 group (Figure. 7c) showed an improvement in bone repair indices compared to the defect group, although the difference was not statistically significant. The indices of bone repair for the MD group (Figure. 7d) were higher than those in the defect group and M0 group, which may be related to the promotion of osteogenic ability of BMSC-exos by mechanical stimulation. The MF group (Figure. 7e) outperformed all three groups in terms of bone repair indices, with statistically significant differences. Furthermore, the structural index (Figure. 7i) in the sheet in MF groups was 1.34 ± 0.13, closer to 1 than that in the other groups, suggesting that the newly formed bone tissue was more mature and closely resembled plate-like bone structure.

The osteoinductive capacity was further assessed through HE staining and Masson staining (Figure. 7j and Figure. k). The results of the HE staining indicated complete degradation of the hydrogel in all groups, with no residual hydrogel observed. Additionally, there were no obvious inflammatory cells observed, suggesting good biocompatibility of the hydrogel and BMSC-exos implant without inducing a significant rejection reaction. Masson staining revealed few blue-stained areas representing new bone tissue in the defect group, slightly more in the M0 group, a substantial amount in the MD groups, and an abundance of new bone tissue as well as red-stained mature bone tissue repairing the bone defect area in the MF groups. These findings suggest that BMSC-exos exhibit stronger osteoinductive ability under mechanical stimulation, particularly under force-controlled loading mode.

Preprint of Bio-Design and Manufacturing (unedited)

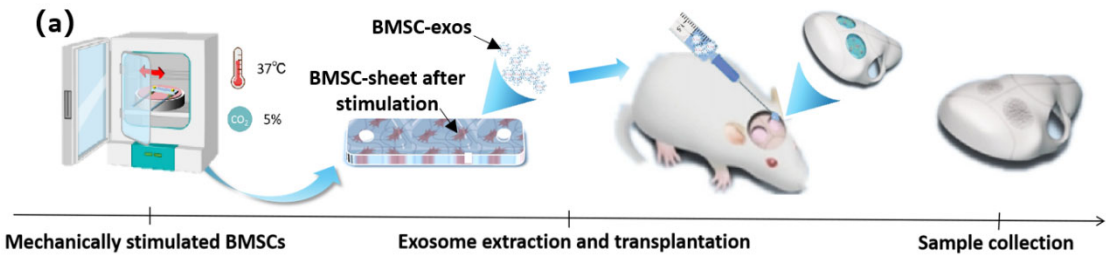

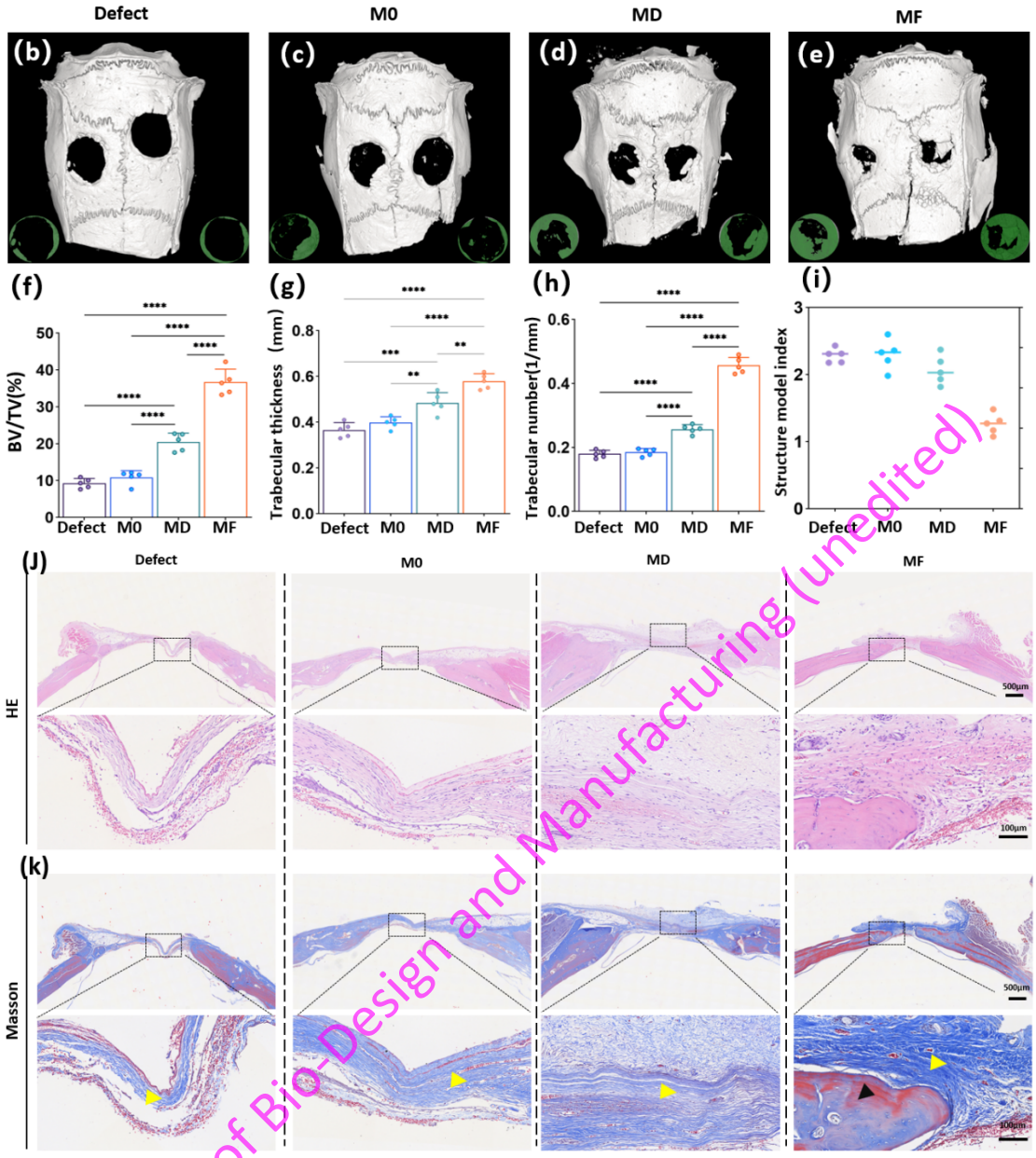

Preprint of Bio-Design and Manufacturing (unedited)

Figure. 7 Repair of bone defect based on the stimulated BMSC-exos. (a) Design of animal experiments; (b-e) Micro CT scan images of skull defects in defect, M0, MD and MF groups, respectively (Green represents newly formed bone tissue). (f-i) Micro CT quantitative statistics of osteogenesis-related parameters for four groups (**P < 0.01; ***P < 0.001; ****P < 0.0001). HE (j) and Masson stain (k) of skull defects of bone regeneration at 8 weeks after surgery in the rat calvarial defect model. (Yellow arrows indicate areas of new bone tissue and black arrows indicate areas of mature bone tissue).

4.Discussion

Exosomes are extracellular vesicles released by cells, containing a variety of bioactive molecules[28,29]. As important signaling molecules, exosomes constitute a novel cell-cell information transmission system, and participate in a variety of biological processes including cell communication, cell migration, angiogenesis, and tumor cell regulation[30]. Most of the functions performed by BMSCs are mediated through BMSC-exos[10]. Furthermore, the

utilization of exosomes circumvents the tumorigenicity associated with stem cell proliferation disorders and offers advantages such as facile transportability and application, direct fusion with target cells to exert biological effects and low immunogenicity[31]. Therefore, cell-free therapy based on exosomes has emerged as a research focus and has been applied to the treatment of a variety of diseases, such as cancer[32], orthopedic diseases[33], chronic refractory wounds[34] and nerve injury[17]. Howerver, The engineering application of exosomes is confronted with the challenge of low yield and reduced biological activity[10]. Various chemical, physical and environmental factors have been explored to enhance the production of exosomes. Physical inductors have received increasing attention due to their advantages over chemical inductors, including higher biosafety and lack of dose dependence[35,36]. Among them, mechanical signaling is an important pathway for cell-cell and cell-environment communication. Therefore, it becomes possible to regulate the secretion of exosomes by mechanical stimulation. Hao et al.[25] developed a novel and high-throughput microfluidic device to permeabilize the cell membrane by applying mechanical squeezing stimulation, which led to an approximately 4-fold increase in the secretion of extracellular vesicles. Additionally, hydrodynamics and stretch stimulation have also been shown to promote the secretion of extracellular vesicles[14,37]. Previous studies on using mechanical stimulation to enhance exosome secretion have mainly focused on 2D culture models[12,14,15]. While this method simplifies research, it significantly differs from the physiological 3D cell growth environment. These dimensional differences critically influence cellular responses to stimuli [16,18,38,39]. Furthermore, 3D culture alone has been shown to enhance the secretion of exosomes, and when combined with mechanical stimulation, there is a synergistic effect that further promotes exosome secretion[40,41]. Therefore, it is crucial to investigate the impact of mechanical stimulation on the secretion of exosomes in a 3D culture environment.

In this study, we explored a force-controlled mechanical loading method suitable for 3D culture. We explored a 3D culture system that was suitable for both BMSCs growth and mechanical stimulation. Synthetic hydrogels, which are capable of mimicking the cellular microenvironment in physiological conditions, play a crucial role in studying cell responses to various physicochemical signals within 3D culture systems[42,43]. It is feasible to obtain the ideal composite hydrogel by blending different hydrogels[44,45]. Our findings suggest that a 3D culture system consisting of 5% GelMA and 0.3% HAMA achieves a balance between cytocompatibility and mechanical properties, which is crucial for prolonged exposure to mechanical loading[26,46]. Among the various mechanical stimuli endured by cells, stretching stimulation has been extensively studied. In 2D cultures, stretching can be easily applied using an elastic culture plate combined with a stretching system[15,37,47]. However, implementing stretching stimulation in a soft hydrogel-based 3D culture system presents challenges. Liu et al.[21,22] developed a deformable membrane platform for mechanically stretching and compressively stimulating cells in a 3D culture system. However, they also noted that their method induces a complex, spatially heterogeneous 3D strain field in the hydrogel, which includes in-plane biaxial tension and through-thickness compression. Therefore, the system cannot be used to accurately control a single strain component, posing a challenge to mechanistic research. Yu et al.[20] constructed a 3D culture environment based on hydrogels and applied mechanical stimulation at 20% strain to investigate the effect of mechanical stimulation on the secreted exos. However, the decay in hydrogel mechanical properties over time means that displacement-controlled loading modes

Preprint of Bio-Design and Manufacturing (unedited)

lead to diminished mechanical stimulation intensity. Real-time mechanical monitoring and feedback adjustments are crucial for maintaining consistent mechanical loading[48]. In this study, we employed innovative mechanical loading systems in conjunction with a long hydrogel sheet-based 3D culture system to ensure spatially homogeneous stretching stimuli. The system's ability to monitor mechanical parameters in real time and perform feedback regulation ensured the consistency of mechanical stimulation during experiments.

Studies have shown that appropriate mechanical stimulation can enhance the proliferation of BMSCs[49,50], while excessive mechanical stimulation can result in cell death[51]. In our study, we observed that all the two stimulation methods we used could significantly promoted cell proliferation, suggesting that the applied stimulation fell within the physiological range. The MF conditions exhibited a greater ability to promote BMSCs proliferation compared to the MD conditions, which was attributed to the force-controlled loading mode that provided continuous and constant cell stimulation throughout the experiment. The enhanced cell proliferation is also advantageous for improving exosome production. Utilizing the force-controled loading system and 3D culture system we developed, we investigated the effect of stretch stimulation on the secretion of BMSC-exos. Our findings revealed that after 7 days of mechanical stimulation, the secretion of BMSC-exos in both MD and MF groups was higher than that in M0 group, indicating that stretch mechanical stimulation effectively promotes BMSC-exos secretion, consistent with previous reports[14,37]. Furthermore, the secretion of exosomes in MF group was the highest. The average exosome secretion from a single cell in the MF group was approximately 3.3 times higher than that in the MD group and 8.5 times higher than that in the M0 group. This indicates that the force-controlled loading mode we utilized had a superior ability to stimulate BMSC-exos secretion. Sequencing and bioinformatics analysis results indicate that mechanical stimulation enhances the interactions between cell-cell and cell-matrix, which is consistent with previous reports[52]. Furthermore, these differentially expressed genes (DEGs) are involved in many key pathways. Therefore, we believe that the gene-level changes induced by mechanical stimulation are crucial for promoting BMSC-exos secretion.In contrast to the gradual decay of displacement-controlled loading during the loading process, force-controlled loading can continuously activate relevant pathways, thus leading to a greater production of exosomes.

Enhancing the function of exosomes is also a research focus. Yan et al.[53] found that mechanical stimulation not only increased the production of exosomes, but also enhanced their ability to repair cartilage defects. The significance of mechanical stimulation in osteogenesis is well documented, with its regulatory effects on BMSCs being extensively explored[35,54-57]. It has been demonstrated that BMSC-exos induced by cyclic mechanical stretch inhibited osteoclast generation and mitigated bone loss caused by mechanical unloading in a hindlimb unloading mouse model by inhibiting the activity of the NF-κB signaling pathway[14]. It has also been reported that 3D culture environment can enhance the osteoinductive ability of MSC-derived exosomes[11,20]. In this study, we further investigated the effect of mechanically stimulated BMSC-exos on the osteogenic differentiation of BMSCs. Our findings indicate that mechanical stimulation induced BMSC-exos could better promote osteogenic differentiation. Notably, the osteogenic effect of the MF group was superior to that of the MD group, which may be attributed to the continuous and stable mechanical stimulation in the MF group. The integration of biologically active materials by loading exosomes is a crucial approach in tissue engineering [33]. Furthermore, pretreatment of cells can lead to obtaining more active exosomes, thereby further

Preprint of Bio Design and Manufacturing (unedited)

improving the functionality of tissue engineering materials[11,31,58]. Our study further investigated whether mechanically loading BMSC-exos could enhance the osteoinductive potential of bone repair materials in vivo. The results indicated that compared to nonstimulated BMSC-exos, the mechanically stimulated BMSC-exos exhibited superior osteoinduction and enhanced bone repair in vivo, highlighting the importance of mechanical stimulation in BMSC tissue engineering. Additionally, our findings also suggest that force-controlled mechanical loading may serve as a novel approach for large-scale production of functionally enhanced BMSC-exos. It is important to note that this study represents a preliminary exploration of the promotion of BMSC-exos secretion and enhancement of their function through force-controlled loading. Further research is necessary to elucidate the relevant mechanisms.

5.Conclusions

To summarize, we employed an innovative mechanical loading system specifically designed for the uniform and consistent mechanical stimulation of cells and successfully applied it to a hydrogel-based 3D culture system. Compared with displacement-controlled loading, force-controlled loading with this system demonstrated a superior ability to promote the secretion of BMSC-exos. Furthermore, BMSC-exos induced by mechanical loading exhibited better osteogenesis ability. The development of this mechanical stimulation system will help overcome the challenges associated with low yield and insufficient functionality in tissue engineering applications of BMSC-exos.

Acknowledgments

The authors are grateful to the funding support from the National Key Research and Development Program of China (2021YFB3802105-3) and the National Natural Science Foundation of China (62173043).

Declaration of Competing Interest

The authors declare that they have no known competing financial interests or personal relationships that could have appeared to influence the work reported in this paper.

References

[1] Tovar N et al., Form and functional repair of long bone using 3D‐printed bioactive scaffolds. J Tissue Eng Regen Med 2018;12:1986-1999.

[2] Rosslenbroich S et al., Current Management of Diaphyseal Long Bone Defects—A Multidisciplinary and International Perspective. J Clin Med 2023;12:6283.

[3] Migliorini F et al., Strategies for large bone defect reconstruction after trauma, infections or tumour excision: a comprehensive review of the literature. Eur J Med Res 2021;26.

[4] Hao J et al., Large-sized bone defect repair by combining a decalcified bone matrix framework and bone regeneration units based on photo-crosslinkable osteogenic microgels. Bioact Mater 2022;14:97-109.

[5] Wang H et al., Construction of Vascularized Tissue Engineered Bone with nHA-Coated BCP Bioceramics Loaded with Peripheral Blood-Derived MSC and EPC to Repair Large Segmental Femoral Bone Defect. ACS Appl Mater Interfaces 2022.

[6] Hoang DM et al., Stem cell-based therapy for human diseases. Signal Transduct Target Ther

Preprint of Bio-Design and Manufacturing (unedited)

2022;7:272-272.
[7] Sissung TM, Figg WD, Stem cell clinics: risk of proliferation. The lancet oncology 2020;21:205-206.
[8] Wang Y et al., Mesenchymal Stem Cell-Derived Extracellular Vesicles in Bone-Related Diseases: Intercellular Communication Messengers and Therapeutic Engineering Protagonists. Int J Nanomedicine 2024;19:3233-3257.
[9] Wu D et al., Bone mesenchymal stem cells stimulation by magnetic nanoparticles and a static magnetic field: release of exosomal miR-1260a improves osteogenesis and angiogenesis. J Nanobiotechnology 2021;19.
[10] Debbi L, Guo S, Safina D, Levenberg S, Boosting extracellular vesicle secretion. Biotechnol Adv 2022;59:107983.
[11] Yu W et al., Higher yield and enhanced therapeutic effects of exosomes derived from MSCs in hydrogel-assisted 3D culture system for bone regeneration. Biomater Adv 2022;133:112646.
[12] Wang Z et al., Cyclic Stretch Force Induces Periodontal Ligament Cells to Secrete Exosomes That Suppress IL-1beta Production Through the Inhibition of the NF-kappaB Signaling Pathway in Macrophages. Front Immunol 2019;10:1310.
[13] Mullen M et al., Mechanical strain drives exosome production, function, and miRNA cargo in C2C12 muscle progenitor cells. J Orthop Res 2023;41:1186-1197.
[14] Xiao F et al., Exosomes derived from cyclic mechanical stretch-exposed bone marrow mesenchymal stem cells inhibit RANKL-induced osteoclastogenesis through the NF-κB signaling pathway. Ann Transl Med 2021;9:798-798.
[15] Lv P et al., Osteocyte-derived exosomes induced by mechanical strain promote human periodontal ligament stem cell proliferation and osteogenic differentiation via the miR-181b-5p/PTEN/AKT signaling pathway. Stem Cell Res Ther 2020;11.
[16] Gupta D, Grant DM, Zakir Hossain KM, Ahmed I, Sottile V, Role of geometrical cues in bone marrow-derived mesenchymal stem cell survival, growth and osteogenic differentiation. J Biomater Appl 2017;32:906-919.
[17] Han M et al., Three-Dimensional-Cultured MSC-Derived Exosome-Hydrogel Hybrid Microneedle Array Patch for Spinal Cord Repair. Nano Lett 2022;22:6391-6401.
[18] Xie M, Zheng Y, Gao Q, He Y, Facile 3D cell culture protocol based on photocurable hydrogels. Biodes Manuf 2021;4:149-153.
[19] Li Y et al., Porous composite hydrogels with improved MSC survival for robust epithelial sealing around implants and M2 macrophage polarization. Acta Biomater 2023;157:108-123.
[20] Yu W et al., Three-dimensional mechanical microenvironment enhanced osteogenic activity of mesenchymal stem cells-derived exosomes. Chem Eng J 2021;417:128040.
[21] Liu H et al., Microdevice arrays with strain sensors for 3D mechanical stimulation and monitoring of engineered tissues. Biomaterials 2018;172:30-40.
[22] Liu H, Usprech J, Sun Y, Simmons CA, A microfabricated platform with hydrogel arrays for 3D mechanical stimulation of cells. Acta Biomater 2016;34:113-124.
[23] Chen X et al., A clamp-free micro-stretching system for evaluating the viscoelastic response of cell-laden microfibers. Biosens Bioelectron 2022;214:114517-114517.
[24] Carroll SF, Buckley CT, Kelly DJ, Cyclic Tensile Strain Can Play a Role in Directing both Intramembranous and Endochondral Ossification of Mesenchymal Stem Cells. Front Bioeng Biotechnol 2017;5.
Preprint of Bio-Design and Manufacturing (unedited)

[25] Hao R et al., Mechanical stimulation on a microfluidic device to highly enhance small extracellular vesicle secretion of mesenchymal stem cells. Mater Today Bio 2023;18:100527.
[26] He J et al., Gelatin Methacryloyl Hydrogel, from Standardization, Performance, to Biomedical Application. Adv Healthc Mater 2023.
[27] Wang M et al., Molecularly cleavable bioinks facilitate high-performance digital light processing-based bioprinting of functional volumetric soft tissues. Nat Commun 2022;13.
[28] Amigorena S, Zitvogel L, Théry C, Exosomes: composition, biogenesis and function. Nature reviews. Immunology 2002;2:569-579.
[29] Raposo G, Stoorvogel W, Extracellular vesicles: exosomes, microvesicles, and friends. The Journal of cell biology 2013;200:373-383.
[30] EL AS, Mager I, Breakefield XO, Wood MJ, Extracellular vesicles: biology and emerging therapeutic opportunities. Nat Rev Drug Discov 2013;12:347-57.
[31] Chen R et al., Evaluating the defect targeting effects and osteogenesis promoting capacity of exosomes from 2D- and 3D-cultured human adipose-derived stem cells. Nano Today 2023;49:101789.
[32] Han QF et al., Exosome biogenesis: machinery, regulation, and therapeutic implications in cancer. Mol Cancer 2022;21:207.
[33] Kang Y et al., Exosome-functionalized magnesium-organic framework-based scaffolds with osteogenic, angiogenic and anti-inflammatory properties for accelerated bone regeneration. Bioact Mater 2022;18:26-41.
[34] Peng H et al., 3D-exosomes laden multifunctional hydrogel enhances diabetic wound healing via accelerated angiogenesis. Chem Eng J 2023;475:146238.
[35] Hao Z et al., Biophysical Stimuli as the Fourth Pillar of Bone Tissue Engineering. Front Cell Dev Biol 2021;9.
[36] Halim A, Ariyanti AD, Luo Q, Song G, Recent Progress in Engineering Mesenchymal Stem Cell Differentiation. Stem Cell Rev Rep 2020;16:661-674.
[37] Guo S et al., Stimulating Extracellular Vesicles Production from Engineered Tissues by Mechanical Forces. Nano Lett 2021;21:2497-2504.
[38] Carter K et al., Characterizing the impact of 2D and 3D culture conditions on the therapeutic effects of human mesenchymal stem cell secretome on corneal wound healing in vitro and ex vivo. Acta Biomater 2019;99:247-257.
[39] Yue M, Liu Y, Zhang P, Li Z, Zhou Y, Integrative Analysis Reveals the Diverse Effects of 3D Stiffness upon Stem Cell Fate. International Journal of Molecular Sciences 2023;24:9311.
[40] Cao J et al., Three-dimensional culture of MSCs produces exosomes with improved yield and enhanced therapeutic efficacy for cisplatin-induced acute kidney injury. Stem Cell Res Ther 2020;11.
[41] Kim M, Yun HW, Park DY, Choi BH, Min BH, Three-Dimensional Spheroid Culture Increases Exosome Secretion from Mesenchymal Stem Cells. Tissue Eng Regen Med 2018;15:427-436.
[42] Loebel C, Mauck RL, Burdick JA, Local nascent protein deposition and remodelling guide mesenchymal stromal cell mechanosensing and fate in three-dimensional hydrogels. Nat Mater 2019;18:883-891.
[43] Huang G et al., Functional and Biomimetic Materials for Engineering of the Three-Dimensional Cell Microenvironment. Chem Rev 2017;117:12764-12850.
[44] Xia H et al., Lyophilized Scaffolds Fabricated from 3D-Printed Photocurable Natural Hydrogel

Preprint of Bio Design and Manufacturing (uncedited)

for Cartilage Regeneration. ACS Appl Mater Interfaces 2018;10:31704-31715.
[45] Gan S et al., Lyophilized Platelet-Rich Fibrin Exudate-Loaded Carboxymethyl Chitosan/GelMA Hydrogel for Efficient Bone Defect Repair. ACS Appl Mater Interfaces 2023;15:26349-26362.
[46] Nedunchezian S et al., Characteristic and Chondrogenic Differentiation Analysis of Hybrid Hydrogels Comprised of Hyaluronic Acid Methacryloyl (HAMA), Gelatin Methacryloyl (GelMA), and the Acrylate-Functionalized Nano-Silica Crosslinker. Polymers (Basel) 2022;14:2003.
[47] Charoenpanich A et al., Cyclic Tensile Strain Enhances Osteogenesis and Angiogenesis in Mesenchymal Stem Cells from Osteoporotic Donors. Tissue Eng Part A 2014;20:67-78.
[48] Qin Y et al., A Stretchable Scaffold with Electrochemical Sensing for 3D Culture, Mechanical Loading, and Real‐Time Monitoring of Cells. Adv Sci (Weinh) 2021;8:2003738.
[49] Hao J et al., Mechanobiology of mesenchymal stem cells: Perspective into mechanical induction of MSC fate. Acta Biomater 2015;20:1-9.
[50] Hung CT, Racine-Avila J, Pellicore MJ, Aaron R, Biophysical Modulation of Mesenchymal Stem Cell Differentiation in the Context of Skeletal Repair. International Journal of Molecular Sciences 2022;23:3919.
[51] Tan J et al., Inhibition of NFkappaB by activated c-Jun NH2 terminal kinase 1 acts as a switch for C2C12 cell death under excessive stretch. Apoptosis 2009;14:764-770.
[52] Sun J et al., "Slow walk" mimetic tensile loading maintains human meniscus tissue resident progenitor cells homeostasis in photocrosslinked gelatin hydrogel. Bioact Mater 2023;25:256-272.
[53] Yan L, Liu G, Wu X, Exosomes derived from umbilical cord mesenchymal stem cells in mechanical environment show improved osteochondral activity via upregulation of LncRNA H19. J Orthop Translat 2021;26:111-120.
[54] Raman N, Imran SAM, Ahmad Amin Noordin KB, Zaman WSWK, Nordin F, Mechanotransduction in Mesenchymal Stem Cells (MSCs) Differentiation: A Review. International Journal of Molecular Sciences 2022;23:4580.
[55] Sun Y et al., Mechanical Stimulation on Mesenchymal Stem Cells and Surrounding Microenvironments in Bone Regeneration: Regulations and Applications. Front Cell Dev Biol 2022;10.
[56] Bandaru P et al., Mechanical Cues Regulating Proangiogenic Potential of Human Mesenchymal Stem Cells through YAP‐Mediated Mechanosensing. Small 2020;16:2001837.
[57] Argentati C et al., Insight into Mechanobiology: How Stem Cells Feel Mechanical Forces and Orchestrate Biological Functions. International Journal of Molecular Sciences 2019;20:5337.
[58] Yuan X et al., Engineering extracellular vesicles by three‐dimensional dynamic culture of human mesenchymal stem cells. J Extracell Vesicles 2022;11.

Preprint of Bio-Design and Manufacturing (uncedited)

Preprint of Bio-Design and Manufacturing (unedited)

Preprint of Bio-Design and Manufacturing (unedited)